

# Light-induced changes in the gap states above midgap of hydrogenated amorphous silicon

P. Kounavis<sup>a)</sup>

Department of Engineering Sciences, School of Engineering, University of Patras, 26504 Patra, Greece

(Received 11 June 2004; accepted 28 September 2004; published online 27 December 2004)

The energy dependence of the capture coefficients and the density of states (DOS) above midgap of hydrogenated amorphous silicon (*a*-Si:H) in annealed and light exposed states are examined by modulated photocurrent experiments. In the annealed and light exposed states, the electrons are found to interact with two different kinds of gap states through trapping and thermal release. The densities of both gap state distributions at trap depths shallower than 0.67 eV below the conduction band decrease rapidly during the initial stage of light degradation. The DOS of the annealed and light exposed states are found to cross at about 0.67 eV. In addition, a parallel increase in the capture coefficients of the gap states at trap depths lower than 0.67 eV is observed indicating a light-induced disorder. The above behavior is explained with the conversion of strained Si-Si and Si-H-Si bonds, which become highly strained during illumination, into dangling bonds near midgap. © 2005 American Institute of Physics. [DOI: 10.1063/1.1823021]

## I. INTRODUCTION

Degradation of the photoelectric properties of hydrogenated amorphous silicon (*a*-Si:H) upon exposure to a strong visible light has remained for many years an unresolved problem. It is of fundamental importance to understand the origin of this phenomenon, which was originally observed as a metastable decay in both the photocurrent and dark current.<sup>1</sup> The photocurrent degradation is thought to arise from the creation of metastable dangling bonds, which is also a characteristic of the light-induced degradation. These dangling bonds are expected to reduce the lifetime of carriers,<sup>2</sup> limiting the performance of solar cells based on *a*-Si:H. However, a good correlation between the defect creation and photocurrent decay<sup>3-5</sup> or solar cells performance<sup>6</sup> was not always observed, raising questions whether the dangling bond creation is the principal problem of the light-induced degradation. Particularly, at the beginning of light exposure a photocurrent decay was observed that was not always followed by a concomitant metastable defect creation.

It is generally assumed that the capture coefficient of the gap states and the mobility of carriers remain essentially unchanged after light irradiation. However, we have observed a metastable light-induced increase in the ratio  $c_n/\mu$  of the effective capture coefficient  $c_n$  to the mobility of carriers  $\mu$  from the modulated photocurrent (MPC) measurements, suggesting an increase in  $c_n$  and/or a decay in  $\mu$ .<sup>5,7</sup> Both a carriers mobility decay and an increase in the capture coefficient of the gap states have been later reported by other experiments<sup>8,9</sup> and may arise from an enhancement of the structural disorder.

The light-induced increase in the effective ratio  $c_n/\mu$  was found to take place before dangling bond creation. Based on this observation, we have earlier proposed<sup>5</sup> that it

is the structural disorder that is first induced while breaking of highly strained bonds follows. Such a light-induced disorder, which is caused by structural changes in many lattice sites exceeding the density of the dangling bonds, was later confirmed by different experiments.<sup>10-13</sup>

Recently, we have applied our improved analysis of the MPC (Ref. 14) to the respective MPC spectra of *a*-Si:H films prepared in different laboratories. From this analysis, two distinct gap state distributions  $D^1(E)$  and  $D^2(E)$  above midgap were commonly deduced having different ratios of the capture coefficients to the carriers mobility  $c_n^1/\mu$  and  $c_n^2/\mu$ .<sup>15</sup> However, we have not examined the capture coefficients  $c_n^1$  and  $c_n^2$  at various trap depths and the respective light-induced changes. In this article, the MPC data measured using various bias light levels in annealed and light exposed states are analyzed. This will provide a more clear evidence of the existence of two different kinds of gap state distributions above midgap, the energy dependence of the capture coefficients and the respective light-induced changes. We concentrate on the initial stage of the light degradation where structural changes are taking place without an apparent defect creation. A relatively low light intensity was used for the light soaking (LS) in order to induce a gradual degradation of the film properties and to record the induced changes in detail. The two gap state distributions  $D^1(E)$  and  $D^2(E)$  above midgap are manifested not only in the *A* state, but also in the light exposed states. The absolute magnitude of each gap state distribution and the energy dependence of the respective capture coefficients are extracted from the analysis of the experimental spectra of the imaginary term of the MPC. The densities of the shallower gap states decrease during the initial stage of LS, while the respective ratios  $c_n^1/\mu$  and  $c_n^2/\mu$  increase. Our results are compared with those reported by other authors and the microscopic mechanism that is compatible with the light-induced changes is discussed.

<sup>a)</sup>Electronic mail: pkounavis@des.upatras.gr

## II. EXPERIMENTAL DETAILS

The *a*-Si:H undoped films were deposited at a substrate temperature of 250 °C by the conventional rf-glow discharge technique at the Energy Conversion Devices. Before LS the samples were annealed at 185 °C for about 2 h and the annealed (A) state was obtained. For the dark current and photocurrent measurements Al electrodes in coplanar configuration were evaporated on the top of the films. A red light of about 10 mW/cm<sup>2</sup> from light emitted diodes (LED's) with a maximum output at about 660 nm was used for the light irradiation. The photocurrent and dark current measurements and the LS were carried out under vacuum at about room temperature (293 K).

The MPC measurements were recorded by employing the frequency resolved spectroscopy to extract the characteristics of the gap states above midgap.<sup>15,16</sup> In this technique, two red LED's (also peaked at 660 nm) were used for the modulated (probe) and constant (bias) band gap light, respectively. The phase shift  $\phi$  and amplitude of the MPC  $i_{ac}$  were measured by a lock-in amplifier as a function of the angular modulation frequency  $\omega$  of the probe light, using various bias light intensities.<sup>7</sup> From these measurements, the imaginary  $Y$  term of the MPC is obtained by means of  $Y = \mu e G_{ac} A \mathcal{E} (\sin \phi / i_{ac})$ , where  $\mu$  is the mobility of the electrons,  $e$  the electronic charge,  $G_{ac}$  the amplitude of the alternating generation rate,  $A$  the conduction cross sectional area of the specimen, and  $\mathcal{E}$  the applied electric field. From the  $Y$  term, the absolute DOS of each probed gap state distribution  $D^i(E)$  and the ratios  $c_n^i/\mu$  of the respective capture coefficients to the carriers mobility are simultaneously extracted.<sup>14-16</sup>

Optical absorption measurements were employed by using the constant photocurrent method (CPM) (Ref. 17) in order to obtain complementary information about the density of the gap states below midgap. A monochromator and a halogen lamp were used for the CPM measurements. The relative values of the subgap absorption from the CPM were fitted on the absolute values of the absorption ( $\alpha \geq 10^4$  cm<sup>-1</sup>) extracted by optical transmission measurements.

The samples were first measured in the A state and subsequently in the light exposed states obtained by successive LS steps. The highest light intensity used for the optical bias was about  $2 \times 10^{14}$  cm<sup>-2</sup> s<sup>-1</sup> in order to prevent light-induced instabilities during the photocurrent measurements. Finally, the samples after the LS cycle were thermally annealed and measured again in order to examine the annihilation of the metastable phenomena and to check whether they are reversible.

## III. RESULTS AND ANALYSIS

### A. The probed defect states

Figure 1(a) presents the imaginary  $Y$  term of the MPC of the A state as a function of the modulation frequency  $\omega$ . A typical example of  $Y$  spectrum in a light exposed state is presented in Fig. 1(b). These spectra are analyzed by assuming that the interaction of electrons with the gap states above midgap through trapping and thermal release predominates

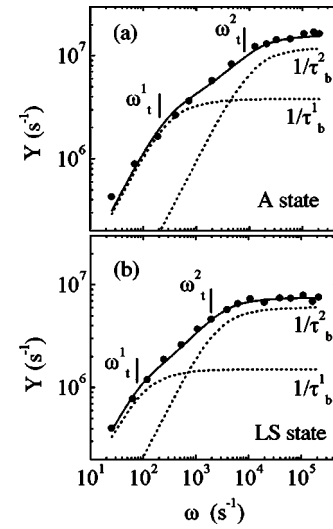


FIG. 1. Experimental imaginary  $Y$  term (points) of the A state in (a) and a light exposed state obtained after 60 min of LS in (b). Calculated effective trapping rates  $1/\tau_b^1$ ,  $1/\tau_b^2$  (dashed lines) into two different kinds of gap state distributions and total effective trapping rates  $1/\tau_b^1 + 1/\tau_b^2$  (solid lines) giving the best fit to the experimental spectra are also included. Arrows indicate the characteristic frequencies  $\omega_1^1$  and  $\omega_1^2$ .

over that of holes with the respective gap states below midgap. In this case, the spectra of  $Y$  term represent the sum of all the effective trapping rates  $1/\tau_b^i$  of electrons<sup>14</sup>

$$Y = \sum_i \frac{1}{\tau_b^i} = \sum_i H^i(\omega, \omega_1^i) c_n^i D^i(E_\omega^i) kT. \quad (1)$$

In the above equation each  $D^i(E_\omega^i)$  is the probed distribution above midgap,  $E_\omega^i$  is the respective probe energy level defined by

$$E_\omega^i = kT \ln \frac{c_n^i N_C}{[\omega^2 + (\omega_1^i)^2]^{1/2}}, \quad (2)$$

where  $\omega_1^i \cong n c_n^i$  is the characteristic frequency,  $c_n^i$  the capture coefficient for electrons,  $n$  the density of free electrons,  $kT$  the thermal energy, and  $N_C \cong 10^{21}$  cm<sup>-3</sup> the effective density of states at the mobility edge where the zero of the energy scale was taken. Each  $H^i(\omega, \omega_1^i)$  function, hereafter  $H^i$  function, is given by

$$H^i(\omega, \omega_1^i) = 1 - \frac{2}{\pi} \arctan \frac{\omega_1^i}{\omega} \quad (3)$$

and determines the effective contribution of each probed gap state distribution  $D^i(E_\omega^i)$  to the  $Y$  term.

Figures 2 and 3 show the characteristic behavior of the  $Y$  spectra upon increasing the bias light intensity. At higher frequencies,  $Y$  is independent of the bias light intensity and this characterizes the emission-limited regime. This regime takes place for  $\omega \gg \omega_1^i$ , where every  $H^i$  function is equal to unity. So the gap states at every probe energy level  $E_\omega^i$  have the maximum effective contribution to the  $Y$  term. This is because the time window corresponding to the modulation period equals the thermal emission time of electrons from each  $E_\omega^i$  level, namely,  $T = 2\pi/\omega = 2\pi/e_n^i(E_\omega^i)$ , where  $e_n^i(E_\omega^i)$  is the thermal emission rate from the  $E_\omega^i$  level. Therefore the contribution of the probed gap states at each  $E_\omega^i$  level to the

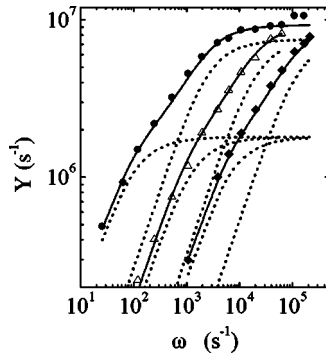


FIG. 2. Experimental imaginary  $Y$  term (points) obtained with various bias light intensities. Solid circles, open triangles, and solid diamonds are the experimental data for a bias light intensity  $1.0 \times 10^{11} \text{ cm}^{-2} \text{ s}^{-1}$ ,  $3.6 \times 10^{12} \text{ cm}^{-2} \text{ s}^{-1}$ , and  $4.6 \times 10^{13} \text{ cm}^{-2} \text{ s}^{-1}$ , respectively. Calculated effective trapping rates  $1/\tau_b^1$ ,  $1/\tau_b^2$  (dashed lines) and total effective trapping rates  $1/\tau_b^1 + 1/\tau_b^2$  (solid lines) that give the best fit to the experimental spectra are also included.

out-of-phase component of the MPC and to the imaginary term due to the thermal interaction of electrons is maximum ( $H^i=1$ ). By changing the modulation frequency for  $\omega \gg \omega_p^i$ , all the probe energy levels  $E_\omega^i$  shift at different energies above the trap quasi-Fermi level of electrons  $E_m$  and the  $Y$  term reflects the DOS distribution in the frequency domain that predominates electron trapping.

At lower frequencies, all the spectra illustrated in the Figs. 2 and 3 represent a decay of  $Y$ , which shifts to higher frequencies upon increasing the bias light level. This behavior is characteristic of the trapping-limited regime, which takes place for  $\omega < \omega_p^i$ . In this regime, the time window corresponding to the modulation period is larger than the thermal emission time from the respective probe energy level, which according to Eq. (2) remains fixed at the  $E_m$  level ( $E_\omega^i \approx E_m$ ), namely,  $T = 2\pi/\omega > 2\pi/e_n^i(E_m)$ . Hence the electrons trapped at  $E_m$  level have a larger available time during a modulation cycle for thermal emission compared to the thermal emission time. Thus the effective contribution of the respective probed distribution  $D^i(E)$  to the out-of-phase component of the MPC and to  $Y$  term is suppressed. This is reflected in the decay of  $H^i$  function by decreasing  $\omega$ .

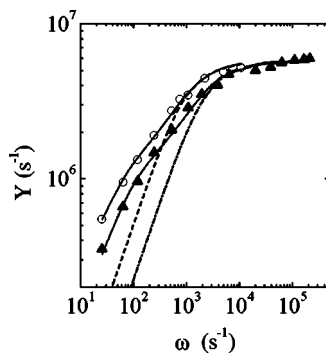


FIG. 3. Experimental imaginary  $Y$  term (points) of two relatively weak bias light intensities  $5.8 \times 10^{10} \text{ cm}^{-2} \text{ s}^{-1}$  (open circles) and  $1.8 \times 10^{11} \text{ cm}^{-2} \text{ s}^{-1}$  (solid triangles). Calculated decay of  $Y$  term assuming a single kind of gap states (broken lines) and total effective trapping rates  $1/\tau_b^1 + 1/\tau_b^2$  (solid lines) that give the best fit to the experimental data.

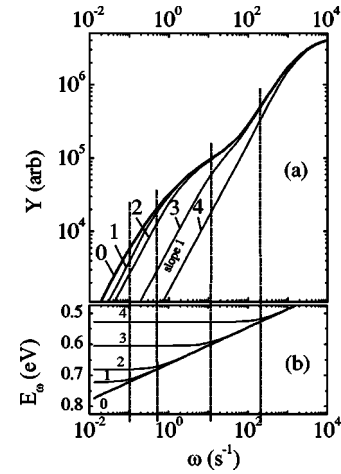


FIG. 4. (a) Calculated imaginary  $Y$  spectra by considering a DOS with two Gaussian gap state distributions and the same capture coefficient. Curve 0 corresponds to an  $E_m$  level near midgap (thick solid line), while curves 1–4 correspond to four shallower  $E_m$  levels respectively (thin solid lines). (b) Evolution of the probe energy  $E_\omega$  level as a function of the modulation frequency  $\omega$ , each plateau at lower  $\omega$  indicates the respective  $E_m$  level.

By assuming that only a single kind of gap state distribution  $D(E)$  is probed, the  $Y$  term in the trapping-limited regime is related only to the respective  $D(E_m)$  at the  $E_m$  level and not to the deeper DOS, as it was usually assumed in the analysis of other authors.<sup>18,19</sup> Upon increasing the bias light level, the  $E_m$  level shifts to shallower states while the characteristic frequency  $\omega_t$  shifts to higher frequencies. Thus the decay of  $Y$  starts to take place from higher frequencies than those with a lower bias light level. The  $Y$  term in the trapping-limited regime ( $\omega < \omega_t$ ) of all the experimental spectra of Figs. 1–3 is expected to have the characteristic linear dependence with decreasing frequency due to the decay of  $H$  function. However, as is shown in Fig. 3, the experimental  $Y$  spectra at lower frequencies are in strong disagreement with the expected linear decay of  $H$  function shown by the respective broken lines. The  $Y$  spectra exhibit a characteristic “stairlike” behavior with two steps taking place at two frequencies that differ by about 1–2 orders of magnitude. These steps were commonly manifested in all the  $Y$  spectra of  $a$ -Si:H samples prepared at different laboratories.<sup>15</sup> Particularly, in some samples these two steps do not overlap and appear more pronounced at well separated characteristic frequencies that differ by more than two orders of magnitude (see Figs. 4 and 6 of Ref. 15).

One may argue that the above stairlike behavior may arise from a structure in the DOS. If this is indeed the case, then one should always observe this structure at the same modulation frequencies independently of the bias light level. However, as can be seen in Figs. 2 and 3 this is not observed. The above predicted behavior of the  $Y$  spectra is demonstrated in detail using the simulated  $Y$  spectra of the example of Fig. 4(a). In this example, two Gaussian gap state distributions are considered to be probed having a maximum density  $1 \times 10^{16} \text{ eV}^{-1} \text{ cm}^{-3}$  and  $3 \times 10^{14} \text{ eV}^{-1} \text{ cm}^{-3}$  at 0.42 eV and 0.55 eV, respectively, below the conduction band. Moreover, the same capture coefficient  $c_n = 1 \times 10^{-8} \text{ cm}^3 \text{ s}^{-1}$  is considered for both distributions. The effect of the bias light

level is studied in the spectra 0–4 of Fig. 4(a) by shifting the trap quasi-Fermi level  $E_m$  at different energy levels. As far as the  $E_m$  level is at deep energies, as in the spectra 0, 1, and 2 of Fig. 4(a), most of the frequencies correspond to the bias light-independent  $Y$  values and to the emission-limited regime ( $\omega \gg \omega_t$ ). In these spectra, the probe energy level  $E_\omega$  calculated from Eq. (2) shifts to different energies above the respective  $E_m$  level by changing the modulation frequency, as is demonstrated graphically in Fig. 4(b). Thus the  $E_\omega$  level shifts between the two Gaussian probed gap state distributions. These two distributions generate a structure in the spectral shape of the calculated  $Y$  spectra, reflecting the structure of the DOS. The structure in the calculated  $Y$  spectra resembles the stairlike structure of Figs. 1–3. However, contrary to the experimental spectra, the structure in the calculated spectra 0, 1, and 2 of Fig. 4(a) appears always at the same frequencies and remains unaffected by the shift of the  $E_m$  level. On the other hand, as is shown with the respective spectra 3 and 4 in Fig. 4(a), the structure in the  $Y$  spectrum gradually disappears by shifting the  $E_m$  level through the region where the DOS structure from the two Gaussian distributions appears. This behavior is observed because most of the frequencies now correspond to the trapping-limiting regime ( $\omega < \omega_t$ ), where  $E_\omega$  is fixed at  $E_m$ . Thus the  $Y$  term reflects the linear decay to zero of the  $H$  function instead of the DOS structure.

The behavior of the experimental spectra upon changing the bias light level is in strong disagreement with that of the calculated spectra of Fig. 4(a). First, the stairlike behavior of  $Y$  term is observed in all the experimental spectra of Figs. 1–3 even in the spectra of Fig. 2 with the higher bias light levels where the trap quasi-Fermi levels have been shifted at shallower states. Second, the two steps do not remain fixed at the same frequencies, but shift almost in parallel to higher frequencies upon increasing the bias light level (see Fig. 2). This shift is observed even in the case where the bias light level is changing in the weakest light intensity regions (see Fig. 3). The above observations rule out the possibility that the characteristic spectral shape of the experimental  $Y$  spectra with the two steps originates from a structure in the gap state distribution.

As we have recently proposed,<sup>15</sup> the  $Y$  spectra of  $\alpha$ -Si:H exhibit all the characteristics of that case where the electrons interact with two different gap state distributions  $D^1(E)$  and  $D^2(E)$  having different capture coefficients  $c_n^1$  and  $c_n^2$ . The two steps indicate the two different characteristic frequencies  $\omega_t^1$  and  $\omega_t^2$  corresponding to the different capture coefficients  $\omega_t^1 \cong nc_n^1$  and  $\omega_t^2 \cong nc_n^2$ . Namely,  $Y$  is given by

$$Y = H^1(\omega, \omega_t^1) c_n^1 D^1(E_\omega^1) kT + H^2(\omega, \omega_t^2) c_n^2 D^2(E_\omega^2) kT. \quad (4)$$

The concept of two different kinds of probed gap states can explain not only the spectral shape with the two steps of the  $Y$  spectra, but also the optical bias dependence of Figs. 2 and 3. This is demonstrated by using the simulated  $Y$  spectra shown in the example of Fig. 5. For simplicity, in our simulations two uniform gap state distributions were considered to be probed above midgap with densities  $D^1(E) = 1 \times 10^{16} \text{ cm}^{-3} \text{ eV}^{-1}$  and  $D^2(E) = 1 \times 10^{15} \text{ cm}^{-3} \text{ eV}^{-1}$  having different capture coefficients  $c_n^1 = 6.3 \times 10^{-9} \text{ cm}^{-3} \text{ s}^{-1}$  and  $c_n^2$

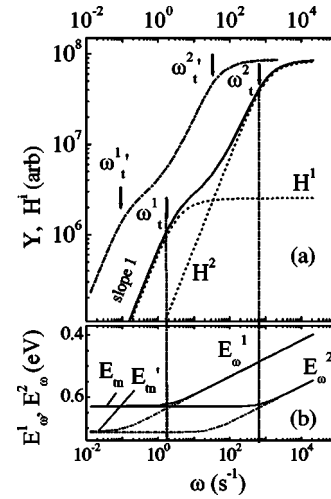


FIG. 5. (a) Calculated imaginary  $Y$  term by considering a DOS with two gap state distributions and two different capture coefficients for a trap quasi-Fermi level at  $E_m = 0.63 \text{ eV}$  (solid line) and  $E_m = 0.72 \text{ eV}$  (dashed-dotted line) below the conduction band. Arrows indicate the respective characteristic frequencies  $\omega_t^i$ . (b) Evolution of the probe energy levels  $E_\omega^1$  and  $E_\omega^2$  as a function of  $\omega$  assuming the trap quasi-Fermi levels at  $E_m = 0.63 \text{ eV}$  (solid lines) and  $E_m = 0.72 \text{ eV}$  (dashed-dotted lines).

$= 2.1 \times 10^{-6} \text{ cm}^{-3} \text{ s}^{-1}$ , respectively. The calculated  $Y$  spectra of Fig. 5(a) represent a clear stairlike behavior with a step at every characteristic frequency  $\omega_t^i \cong nc_n^i$  marked by the arrows. Every step in  $Y$  spectra reflects the characteristic spectral shape of  $H^i$  function, which is a step function. The step takes place at the characteristic frequency  $\omega_t^i$ , whereas in the region of  $\omega < \omega_t^i$   $H^i$  function decays linearly with decreasing  $\omega$ , as is graphically demonstrated in Fig. 5(a) (dotted lines). As can be seen in Fig. 5(b), a given trap quasi-Fermi level of electrons  $E_m$  corresponds to two different characteristic frequencies  $\omega_t^1$  and  $\omega_t^2$  for the  $D^1(E)$  and  $D^2(E)$  distributions, respectively. By decreasing the frequency in the region of  $\omega < \omega_t^2$ , the probe energy level  $E_\omega^2$  remains fixed at the  $E_m$  level. Thus the  $H^2$  function and the effective trapping rate into the  $D^2(E)$  decays rapidly making apparent the effective trapping rate into the other  $D^1(E)$  distribution with the lower capture coefficient. Upon decreasing the bias light level, the  $E_m$  level shifts to deep energies and the two steps in the  $Y$  shift in parallel to low frequencies,  $\omega_t^{1'}$  and  $\omega_t^{2'}$  in Fig. 5(a). This is qualitatively a very similar behavior to that observed experimentally (see Figs. 2 and 3) and can be taken as a manifestation that the decay of  $Y$  at every  $\omega_t^i$  arises from the suppression of the respective effective trapping rate  $1/\tau_b^i = H^i(\omega, \omega_t^i) c_n^i D^i(E_\omega^i) kT$ . It must be emphasized that we have observed two obvious steps in the  $Y$  spectra, representing the same characteristic behavior by changing the bias light level in all the examined undoped  $\alpha$ -Si:H films. These films have been deposited under different deposition conditions, such as various substrate temperatures, interelectrode spacing, rf powers, gas flow rates using either silane or disilane with or without H, He, Ar dilution etc.

As the probe energy level remains practically at the  $E_m$  level for  $\omega \ll \omega_t^i$  [see Fig. 5(b)], the absolute magnitude of the  $Y$  term at around  $\omega_t^i$  is practically determined from the probed DOS  $D^i(E_m)$ , whereas the decay of  $Y$  at lower  $\omega$  is governed by the decay of the  $H^i$  function. Thus, by adjusting

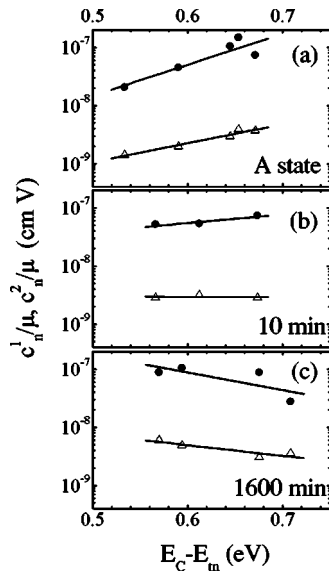


FIG. 6. The extracted ratios  $c_n^1/\mu$  (open triangles) and  $c_n^2/\mu$  (closed circles) as a function of the  $E_m$  level of the A state in (a) and two LS states obtained with the indicated illumination times in (b) and (c). Solid lines represent the exponential variations  $c_n^i = c_0^i \exp(E/E_0^i)$  for  $c_n^1$  and  $c_n^2$ .

the absolute values of  $D^1(E_m)$ ,  $D^2(E_m)$ ,  $\omega_t^1$ , and  $\omega_t^2$ , the  $Y$  spectra that give the best fits to the experimental spectra are calculated by using Eqs. (3) and (4). The so-calculated  $Y$  spectra (solid lines) of Figs. 1–3 make always a good fit to the respective experimental spectra (points).

## B. The energy dependence of the capture coefficients and DOS

The values of  $\omega_t^i$ , as determined above from the fit of the experimental  $Y$  spectra, are used to determine each ratio  $c_n^i/\mu$  of the capture coefficient of the probed gap states at the respective  $E_m$  level to the carriers mobility using  $c_n^i/\mu = e\omega_t^i/\sigma_p$ , where  $\sigma_p$  is the dc photoconductivity. Upon changing the bias light level, the two steps in the  $Y$  term and the respective  $\omega_t^i$  shift to different modulation frequencies and trap depths. In this way, information can be deduced about the energy dependence of the capture coefficients.

Figure 6 presents the extracted ratios  $c_n^1/\mu$  and  $c_n^2/\mu$  of the two probed  $D^1(E)$  and  $D^2(E)$  distributions as a function of  $E_m$  level of the A state in (a) and two light exposed states in (b) and (c). The  $E_m$  level was approximated by the quasi-Fermi level  $E_{Fn}$  of free electrons as calculated from dc photoconductivity. As can be seen in Fig. 6(a), both ratios  $c_n^1/\mu$  and  $c_n^2/\mu$  of the A state increase with the increase of the trapping energy, suggesting a nearly exponential energy dependence  $c_n^i = c_0^i \exp(E/E_0^i)$  for the capture coefficients  $c_n^1$  and  $c_n^2$  with characteristic energies  $E_0^1 \approx 130$  meV and  $E_0^2 \approx 80$  meV, respectively.

Since our basic analysis has been developed for energy independent capture coefficients, it could be inappropriate for our case where there is such an energy dependence. This is because by changing  $\omega$  around the characteristic frequency  $\omega_t$  and lower frequencies, the respective probe energy level has a minor shift close to the  $E_m$  level [see Fig. 4(b)]. Thus a possible energy dependence of the capture coefficients may affect the decay of  $Y$  at the characteristic frequencies. In fact,

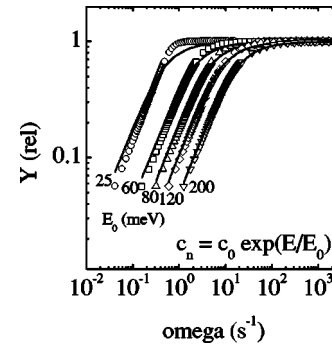


FIG. 7. Net decay of the  $Y$  term (symbols) due to the decay of  $H$  function as calculated from Eq. (3) assuming a capture coefficient having an exponential variation  $c_n = c_0 \exp(E/E_0)$  and the indicated characteristic energies  $E_0$ . The respective net decay of the  $Y$  term calculated for an energy independent capture coefficient is also included for comparison (solid lines).

this is expected to have a minor effect in  $Y$ , providing that the energy dependence of the capture coefficients is not strong. This is demonstrated here with the aid of simulations. The net decay of  $Y$  term at lower frequencies from the decay of  $H$  function was calculated by using Eq. (3) and considering an energy dependent capture coefficient  $c_n = c_0 \exp(E/E_0)$  with various characteristic energies  $E_0$ . The so-calculated spectra are plotted in Fig. 7 (symbols), along with those calculated assuming an energy independent  $c_n$  (lines) for comparison. From this figure, it is evident that, when  $c_n$  has a relatively weak exponential dependence with a characteristic energy in a region of  $E_0 \geq 80$  meV, which includes both the observed values  $E_0^1$  and  $E_0^2$ , the calculated net decay of  $Y$  term around  $\omega_t$  is always practically very close to that obtained for an energy independent capture coefficient.

Therefore, as long as the energy dependence of  $c_n$  is relatively weak, as in our case, then the respective decay of  $Y$  is not significantly affected by this dependence and our analysis can be safely applied to extract the ratios  $c_n^i/\mu$ . As is also shown in Fig. 7, the calculated decay of  $Y$  deviates from that found for an energy independent capture coefficient only for the cases characterized by a steep energy dependence of  $c_n$  with  $E_0 < 80$  meV. In these cases, the  $Y$  spectra cannot be fitted by assuming an energy independent capture coefficient.

Upon LS, both ratios  $c_n^1/\mu$  and  $c_n^2/\mu$  demonstrated in Figs. 6(b) and 6(c) represent an increase in energies shallower than 0.6–0.65 eV, while these ratios slightly decrease for the deep energies around 0.7 eV. As a result, the energy dependence of the above ratios become almost flatlike in the light exposed states, indicating that the capture coefficients become nearly energy independent.

The  $D^1(E)$  and  $D^2(E)$  distributions in the A state and two light exposed states, as determined from the fitting process of the  $Y$  spectra of various bias light levels, are shown in Fig. 8 as a function of the  $E_m$  level. It can be seen that in every state the relative density of the above two distributions differ by about an order of magnitude. The DOS of both  $D^1(E)$  and  $D^2(E)$  distributions at shallower energies than about 0.67 eV decreases upon LS, whereas the deep DOS at about 0.7 eV shows a trend to increase. As a result of these changes, a crossing between the DOS of the A state and that of the light exposed states appears at about 0.67 eV. In addition, as can

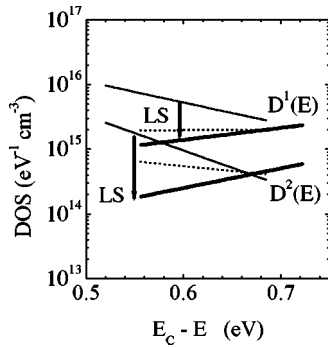


FIG. 8. DOS of  $D^1(E)$  and  $D^2(E)$  distributions in the A state (thin solid lines) and two LS states obtained with 10 min (dashed lines) and 1600 min (thick solid lines) of light irradiation.

be seen in Fig. 8, most of the changes in the DOS were induced during the first 10 min of the initial stage of LS.

### C. Evolution of the light-induced changes

The detailed evolution with the LS time of the ratios  $c_n^1/\mu$ ,  $c_n^2/\mu$ , and  $D^1(E)$ ,  $D^2(E)$  at a trap depth of 0.55 eV is shown in Figs. 9(a) and 9(b), respectively. As can be seen in these figures, after the initial stage of LS, the changes in the DOS were induced with a relatively slower rate.

The evolution with LS time of the subgap absorption  $\alpha_{1,3}$  at photon energy  $E=1.3$  eV from the CPM is shown in Fig. 9(c). The subgap absorption  $\alpha_{1,3}$  as well as the whole subgap absorption at photon energies in the region of 0.8–1.5 eV (not shown) remained fixed during the initial stage of LS. The subgap absorption  $\alpha_{1,3}$ , which is considered as a measure of the dangling bond density below midgap, requires more than 60 min of LS to increase. Thus, from the constant subgap absorption at the beginning of LS, a constant dangling bond density can be concluded. A similar conclusion was deduced by Nadazdy *et al.*<sup>20</sup> from charge deep level transient spectroscopy (Q-DLTS) measurements. From these measurements the extracted neutral dangling bond den-

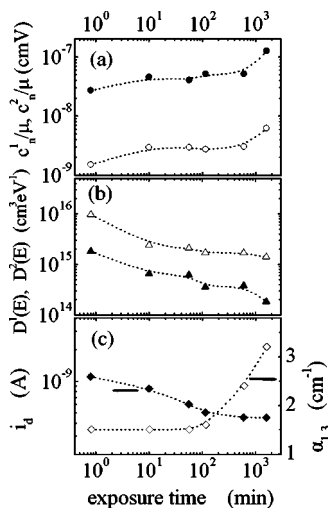


FIG. 9. Evolution as a function of the illumination time of the ratios  $c_n^1/\mu$  (open circles),  $c_n^2/\mu$  (closed circles) in (a), absolute values of  $D^1(E)$  (open triangles),  $D^2(E)$  (closed triangles) distributions at 0.55 eV in (b), and subgap absorption  $\alpha_{1,3}$  (open diamonds and right axis), dark current  $i_d$  (closed diamonds and left axis) in (c). Lines serve as guide to the eye.

sity was found to be constant during the first several minutes of LS increasing at longer times in parallel with the electron spin resonance (ESR) signal.<sup>20</sup> Moreover, we have found that the LS time, during which the subgap absorption was practically constant, became shorter by using a stronger light irradiation intensity.<sup>5</sup>

Although during the initial stage of LS the dangling bond density is constant, the dc photocurrent is found to decay.<sup>5,7</sup> In addition, most of the light-induced decay in the dark current occurs during the initial stage of LS, as can be seen in Fig. 9(c).

All the light-induced changes in the MPC were found to be reversible upon thermal annealing. After heating at 185 °C a full recovery of all the measured properties was achieved.<sup>7</sup>

## IV. DISCUSSION

### A. Comparison to the results of other authors

The calculated DOS above midgap according to the defect pool model more likely corresponds to the positively charged dangling bonds  $D^+$ .<sup>21–23</sup> Their density was predicted to increase upon LS along with the neutral dangling bond density. However, this prediction does not agree to the decay of the DOS of Fig. 8. Such an unexpected decay of the DOS above midgap has been also deduced recently from the analysis of the Q-DLTS signal at low temperatures by Nadazdy *et al.*<sup>20</sup> These authors claimed that the decay of the DOS is due to the removal of the positively charged  $D^+$  dangling bonds, producing the shift of the Fermi level towards midgap and the decay of the dark current and photocurrent. This interpretation could be supported from the parallel changes in the DOS above midgap and dark current  $i_d$  at the beginning of LS [see Figs. 9(b) and 9(c)].

The light-induced changes in the DOS of Fig. 8 is also in very good agreement with the respective changes in the DOS above midgap reported by Schumm *et al.*<sup>24</sup> and Georguieva *et al.*<sup>25</sup> using MPC measurements as well. The above authors found that the defect density at the shallower states decreases, while that near midgap increases with LS. Thus the DOS before and after the LS represents a crossing that is also seen in our DOS at about 0.67 eV of Fig. 8. A similar behavior with a crossing in the DOS was obtained by post transient photocurrent (TPC) experiments.<sup>26,28</sup>

It is worthwhile to notice that in the calculated light-induced changes of the DOS from MPC and TPC experiments reported earlier by different authors, various simplifying assumptions have been made. Specifically, it was assumed a single capture coefficient of the probed states for the whole energy range remained unaffected by the LS. Moreover, the possible existence of different kinds of gap states with different capture coefficients was neglected. Thus, if the capture coefficients are considered to increase upon LS in the analysis of the TPC measurements, then the calculated light-induced decay of the DOS should be stronger than that reported in Refs. 26 and 28. Similarly, the light-induced increase of the DOS, usually calculated by other authors from the analysis of MPC measurements,<sup>18</sup> may arise from an increase in the capture coefficients, which were assumed

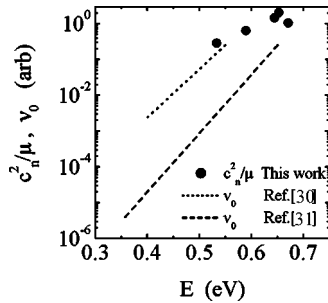


FIG. 10. Variation with trap depth energy of the ratio  $c_n^2/\mu$  (closed symbols) of the  $A$  state and attempt-to-escape frequency  $\nu_0$  from Ref. 30 (dotted line) and Ref. 31 (dashed line).

*a-priori* constant.

In the present work, the capture coefficients of the two probed gap state distributions are studied systematically in the  $A$  and light exposed states as a function of the trap depth energy. This allows us to determine the absolute DOS distribution, the energy dependence of the capture coefficients, and the induced changes by LS. As can be seen from the data of the  $A$  state in Fig. 6(a), the capture coefficients increase with the trap depth. A qualitatively similar dependence was found for the attempt-to-escape frequency  $\nu_0$ , extracted from the TPC experiments of Yan and Adriaenssens,<sup>30</sup> Antoniadis and Schiff.<sup>31</sup> Their results are plotted in Fig. 10. It is known that the  $\nu_0$  is the product of the  $N_C$  and capture coefficient  $c_n$  of the gap states predominating electron trapping in the TPC ( $\nu_0 = c_n N_C$ ). According to our analysis, the  $D^2(E)$  distribution dominates electron trapping. Thus, the  $\nu_0$  from TPC is reasonable to be compared with the ratio  $c_n^2/\mu$  that is also included in Fig. 10. As it can be seen from this figure, both  $\nu_0$  and  $c_n^2/\mu$  represent a similar trend and increase with the trap depth, supporting an energy dependence for the capture coefficients. The relatively stronger energy dependence of  $\nu_0$  could be due to an additional possible temperature dependence, as it has been extracted from various temperatures, while the  $c_n^2/\mu$  are extracted here from a single temperature (293 K) only.

The light-induced increase of the ratios  $c_n^1/\mu$  and  $c_n^2/\mu$  (Fig. 6) may arise from an increase of the capture coefficients and/or a decay of the carriers mobility. A relatively small decay of the carriers mobility has been reported by the photomixing technique during LS.<sup>8</sup> However, only a decay in the mobility is expected rather to cause a uniform increase of the above ratios of Fig. 6 in all the probed energies, instead of the observed pronounced increase at trap depths shallower than 0.6–0.65 eV. Then, it is more reasonable to conclude that it is the capture coefficients  $c_n^1$  and  $c_n^2$  of the shallow gap states that mainly increase. An increase of the capture coefficients upon LS was also reported by photoconductivity and space charge relaxation experiments.<sup>9</sup> Therefore the light-induced increase of  $c_n^1/\mu$  and  $c_n^2/\mu$  can be attributed to an increase of the structural disorder that mainly affects the trapping probability through the enhancement of the phonon coupling, which is expected to greatly facilitate the trapping and thermal release of the electrons. Indeed, such an effect characterized by a dramatic increase in the thermal emission

rate prefactor was found from DLTS upon enhancing the structural randomness by increasing the Ge content in relaxed Si-Ge alloys.<sup>27</sup>

Hattori *et al.*<sup>18</sup> also studied the light-induced changes both in the DOS and in capture coefficients from MPC measurements recorded using the bias light level spectroscopy. The above authors also found two different kinds of gap state distributions  $D^1(E)$  and  $D^2(E)$  above midgap. They found that the density of these distributions increase upon LS without, however, reporting anything about systematic changes in the values of the capture coefficients  $c_n^1$  and  $c_n^2$ , which were found in the regions of  $(0.3-1.4) \times 10^{-8} \text{ cm}^3 \text{ s}^{-1}$  and  $(0.8-1.4) \times 10^{-6} \text{ cm}^3 \text{ s}^{-1}$ , respectively.

Light-induced changes in the capture coefficients can be deduced from the respective changes in the attempt-to-escape frequency  $\nu_0$  reported by Sakata and Yamanaka<sup>28</sup> using TPC measurements. These authors studied the changes in  $\nu_0$ , but only of the deep gap states. They found a small decrease of  $\nu_0$  from  $3.6 \times 10^{13} \text{ s}^{-1}$  to  $1.6 \times 10^{13} \text{ s}^{-1}$  at 0.75 eV below the conduction band after LS, which qualitatively agrees with the respective decrease of  $c_n^1/\mu$  and  $c_n^2/\mu$  for the deeper gap states at about 0.7 eV of Fig. 6.

Okushi *et al.* reported a significant light-induced increase by an order of magnitude in the electron capture cross section of  $P$ -doped  $a$ -Si:H films from isothermal capacitance transient spectroscopy.<sup>29</sup> These authors also found that in the lightly doped samples (0.01% P) the observed increase of the capture cross section was not followed by the creation of metastable defects.

## B. Identification of the probed defects

Based on the large difference of the capture coefficients of the two kinds of probed gap state distributions above midgap, we have recently assigned them into dangling bonds having different atomic configurations.<sup>15</sup> The  $D^2(E)$  distribution with the higher capture coefficient was attributed to dangling bonds with a Si-H back bond. The other  $D^1(E)$  distribution with the lower capture coefficient was attributed to normal dangling bonds without a H atom next to them. This interpretation is in agreement with the fact that most of the dangling bonds are formed in the H depleted regions,<sup>32</sup> since the density of  $D^1(E)$  is higher than that of  $D^2(E)$ . Moreover, the Si-H bond has a stretching mode of vibration of  $2000 \text{ cm}^{-1}$  and corresponds to a phonon energy of 0.25 eV, which is much higher than that of 0.06 eV of the normal Si-Si bonds. The relatively higher vibration mode of Si-H bond can quantitatively provide the much larger capture probability of the  $D^2(E)$  compared to that of  $D^1(E)$  distribution.<sup>15</sup>

The  $D^2(E)$  distribution with the higher capture coefficient can be alternatively attributed to other H related defects. Theoretical calculations showed that H in interstitial sites (Si-H-Si), known as three center bonds (TCB), introduce energy levels in the upper half of the energy gap in the region probed by the MPC. The TCB have also a relatively high frequency of stretching mode of vibration in the region of  $1900-2200 \text{ cm}^{-1}$ , which can also provide a relatively high capture probability for the carriers. The interstitial H is be-

lieved to play an important role in the light degradation mechanism of *a*-Si:H. Upon illumination, H may migrate from a bond center to another bond center site and subsequently retrap into Si–H bonds and dangling bonds.<sup>33</sup> Thus, a depletion of the TCB upon LS is expected, which can explain, in general, the decay of  $D^2(E)$ .

The interstitial H has been manifested in *c*-Si in the bond center configuration and it has been identified as a donor energy level at 0.2 eV below the conduction band.<sup>34,35</sup> Fisch and Licciardello<sup>36</sup> proposed that the interstitial H also exists in *a*-Si:H in the colinear configuration, introducing defect energy levels in the upper half of the energy gap. Biswas *et al.*, by applying tight-binding electronic structure calculations in *a*-Si:H models, concluded that the interstitial H remains off-center in a bridged configuration, having an unoccupied energy level in the upper half of the energy gap.<sup>37</sup>

An initial density of TCB, which can be frozen in during the growth process, is reasonable to exist in the samples of the *A* state.<sup>36–38</sup> The origin of the TCB is probably due to the H atoms from the growth flux which may insert in strained (Si–Si) bonds at the growing film surface releasing strains.<sup>39</sup> Therefore the TCB are very possible candidates for the  $D^2(E)$  distribution.

### C. The microscopic mechanism of the light-induced changes

Since the decay of the DOS above midgap upon LS has been deduced not only from MPC experiments, but also from other experimental techniques like TPC and Q-DLTS, each one with different limitations, it is more likely an inherent property of *a*-Si:H. This decay of the DOS along with the respective crossing near midgap may arise, in general, from conversion of the shallow gap states into deep ones upon illumination. Either the weak bond to dangling bond-breaking conversion models or the charged dangling bond model, in general, can explain this behavior.

The weak bond to dangling bond-breaking conversion models can be combined with the light-induced increase of the structural disorder deduced from the increase of the respective ratios  $c_n^1/\mu$  and  $c_n^2/\mu$ . Specifically, as we have earlier proposed,<sup>5</sup> the energy released from the recombination of the light-induced electrons and holes may cause bond angle and bond length distortions, accumulating strains in some lattice sites. Thus, some weak or strained bonds at shallow energy levels become highly strained and eventually break producing dangling bonds near midgap. This mechanism is reasonable to explain the decay of  $D^2(E)$  distribution because, as mentioned above, it could be attributed to TCB arising from the insertion of H into strained Si–Si bonds. In this case, the decay of  $D^2(E)$  indicates the elimination of TCB as these bonds may break upon LS.

Since the  $D^1(E)$  distribution demonstrates a very similar behavior with that of  $D^2(E)$  and also decays upon LS, then more likely it could be attributed to antibonding states of strained Si–Si bonds located in H depleted regions. If a highly strained Si–Si bond breaks, then a pair of dangling bonds is formed, which is unstable because bond reformation may take place. Besides this, pulsed ESR measurements

showed that most of the native or the light-created dangling bonds are well separated from each other.<sup>32</sup> Thus isolated dangling bonds should be produced after bond breaking. This may be accomplished by the formation of a pair of a dangling bond and a floating bond.<sup>40,41</sup> Specifically, following bond breaking, one of the Si atoms could be threefold coordinated, that is a normal dangling bond. The other Si atom could be fivefold coordinated with a Si atom from the third nearest neighbors. The fivefold coordinated Si atom is a floating bond that can move via bond switching process.<sup>42</sup> The floating bond finally could be converted into a dangling bond at a lattice site away from the other dangling bond, for example, by involving a local motion of H as described in the model of Biswas *et al.*<sup>43</sup>

In the case of the Si–H–Si bonds, as the structural disorder increases upon illumination, these bonds are elongated. In such a case, according to *ab initio* calculations<sup>44</sup> the H atom may be displayed closer to the one Si atom forming a strong Si–H bond. Thus an unpaired electron is left on the other Si atom, which looks like a normal dangling bond near midgap. Although the above created dangling bonds have a H next to them, this does not contradict the limitation imposed by the pulsed ESR measurements, which imply that the majority of the native and light created dangling bonds are formed in the H depleted regions.<sup>32</sup> Indeed, according to our interpretation the expected density of the resulting dangling bonds with a H atom next to them, as estimated from the decay of  $D^2(E)$  distribution of Fig. 8, is much lower than the expected density of the created normal dangling bonds estimated from the respective decay of  $D^1(E)$  distribution.

In the charged defect model,<sup>45</sup> conversion of shallow to deep states is also predicted. This is accomplished by trapping of carriers into charged diamagnetic dangling bonds ( $D^+$ ,  $D^-$ ) at shallow energy levels, converting them into deep paramagnetic dangling bonds ( $D^0$ ). The decay and the crossing of the  $D^1(E)$  and  $D^2(E)$  distributions can be reconciled with this model if both distributions at shallower states could be attributed to positively charged dangling bonds. Indeed, assuming the widely accepted mobility  $\mu=10$  Vs/cm<sup>2</sup>, the two ratios  $c_n^1/\mu$  and  $c_n^2/\mu$  of Fig. 6 give  $c_n^1 > 10^{-8}$  cm<sup>3</sup>/s and  $c_n^2 > 10^{-7}$  cm<sup>3</sup>/s, that are reasonable for positively charged gap states. The difference between the order of magnitude of  $c_n^1$  and  $c_n^2$  can be attributed to a different local atomic configuration of the respective gap states, as explained in the previous section.

The light-induced decay and the crossing observed in the  $D^1(E)$  distribution could be due to the conversion of the positively charged dangling bonds at shallower states into neutral ones near midgap. The charged dangling bonds may originate from negative effective electronic correlation energy  $U_{eff}$ <sup>45</sup> or potential fluctuations.<sup>46</sup> A similar conversion mechanism with that reported above for diamagnetic dangling bonds can be also applied to the other  $D^2(E)$  distribution, which was attributed in the previous section to TCB also characterized by negative- $U_{eff}$  properties.<sup>36</sup> Indeed, Biswas *et al.*<sup>37</sup> by using molecular dynamics simulations predicted that under illumination positively charged defects, associated with the bond bridged H centers, could be converted into deeper neutral dangling bonds with the capture of an

electron and a consequent decrease in the dark conductivity. This process could be supported from the decay of both the DOS above midgap and dark current [see Figs. 9(b) and 9(c)].

A serious drawback with the charged defect model is the fact that this model cannot be reconciled with the energy dependence of the capture coefficients. Specifically, the DOS near midgap should correspond to the neutral defects, whereas that at shallow energies to charged defects. Thus the capture coefficient of the deep states is expected lower than that of shallow states, which is not experimentally observed. In fact, the opposite behavior is revealed from the data of the *A* state in Fig. 6(a), where the capture coefficients of the gap states near midgap found higher than those of the shallow energy levels. Therefore the weak bond to dangling bond-breaking conversion models appear more favorable to interpret our results.

## V. CONCLUSION

Two kinds of gap state distributions  $D^1(E)$  and  $D^2(E)$  were manifested above midgap not only in the *A* state, but also in the light exposed states. The respective densities of these two probed distributions, that are shallower than about 0.67 eV below the conduction band, decrease upon LS. Each DOS distribution after LS represents a crossing with the respective one of the *A* state at about 0.67 eV. Both ratios  $c_n^1/\mu$  and  $c_n^2/\mu$  of the shallower energies increase upon LS, suggesting a light-induced increase in the structural disorder of the shallower gap states. The decay and the crossing in the DOS indicate conversion of shallower states into deeper ones near midgap. The observed decay of  $D^1(E)$  and  $D^2(E)$  distributions can be attributed to the elimination of strained Si–Si and Si–H–Si bonds, respectively. These bonds probably become highly strained during LS and eventually break producing dangling bonds near midgap.

## ACKNOWLEDGMENTS

The author is grateful to S. R. Ovshinsky, R. T. Young of Energy Conversion Devices (ECD), and E. Mytilineou for providing the samples.

<sup>1</sup>C. R. Wronski, Mater. Res. Soc. Symp. Proc. **467**, 7 (1997).

<sup>2</sup>M. Stutzmann, W. B. Jackson, and C. C. Tsai, Phys. Rev. B **32**, 23 (1985).

<sup>3</sup>D. Han and H. Fritzsche, J. Non-Cryst. Solids **59/60**, 397 (1983).

<sup>4</sup>H. R. Park, J. Z. Liu, and S. Wagner, Appl. Phys. Lett. **55**, 2658 (1989).

<sup>5</sup>P. Kounavis, J. Appl. Phys. **77**, 3872 (1995).

<sup>6</sup>J. Pearce, X. Niu, R. Koval, G. Gangluly, D. Carlson, R. W. Collins, and C. R. Wronski, Mater. Res. Soc. Symp. Proc. **664**, A12.3 (2001).

<sup>7</sup>P. Kounavis and E. Mytilineou, J. Phys.: Condens. Matter **11**, 9105 (1999).

<sup>8</sup>Y. Tang and R. Braunstein, J. Appl. Phys. **79**, 850 (1996).

<sup>9</sup>M. Meaudre and R. Meaudre, J. Phys.: Condens. Matter **13**, 5663 (2001).

<sup>10</sup>D. P. Masson, A. Ouhlal, and A. Yelon, J. Non-Cryst. Solids **190**, 151 (1995).

<sup>11</sup>Y. P. Zhao, D. L. Zhang, G. L. Kong, G. Q. Pan, and X. B. Lia, Phys. Rev. Lett. **74**, 558 (1995).

<sup>12</sup>T. Gotoh, S. Nonomura, M. Nishido, and S. Nitta, Appl. Phys. Lett. **72**, 2978 (1998).

<sup>13</sup>K. Shimizu, J. Non-Cryst. Solids **266/269**, 486 (2000).

<sup>14</sup>P. Kounavis, Phys. Rev. B **64**, 045204 (2001).

<sup>15</sup>P. Kounavis, Phys. Rev. B **65**, 155207 (2002).

<sup>16</sup>P. Kounavis, Recent Res. Devel. Physics **77**, 773 (2003).

<sup>17</sup>P. Kounavis and E. Mytilineou, Philos. Mag. Lett. **72**, 117 (1996).

<sup>18</sup>K. Hattori, M. Anzai, H. Okamoto, and Y. Hamakawa, J. Appl. Phys. **77**, 2989 (1995).

<sup>19</sup>C. Longeaud, D. Roy, and O. Saadane, Phys. Rev. B **65**, 085206 (2002).

<sup>20</sup>V. Nadazdy, R. Durny, I. Thurzu, E. Pincik, A. Nishida, J. Shimizu, M. Kumeda, and T. Shimizu, Phys. Rev. B **66**, 195211 (2002).

<sup>21</sup>M. J. Powel and S. C. Dean, Phys. Rev. B **48**, 10815 (1993).

<sup>22</sup>G. Schumm, Phys. Rev. B **49**, 2427 (1988).

<sup>23</sup>M. J. Powel and S. C. Dean, Phys. Rev. B **53**, 10121 (1996).

<sup>24</sup>G. Schumm, K. Nitsch, and G. H. Bauer, Philos. Mag. B **58**, 411 (1998).

<sup>25</sup>M. Gueorguieva, C. Main, and S. Reynolds, Mater. Res. Soc. Symp. Proc. **664**, A19.3.1 (2001).

<sup>26</sup>B. Yan, D. Han, and G. J. Adriaenssens, J. Appl. Phys. **79**, 3597 (1996).

<sup>27</sup>A. Mesli and A. Nylandsted Larsen, Phys. Rev. Lett. **83**, 148 (1998).

<sup>28</sup>I. Sakata and M. Yamanaka, J. Appl. Phys. **94**, 3185 (2003).

<sup>29</sup>H. Okushi, M. Miyakawa, Y. Tokumaru, S. Yamasaki, H. Oheda, and K. Tanaka, Phys. Rev. Lett. **42**, 895 (1983).

<sup>30</sup>B. Yan and G. J. Adriaenssens, J. Appl. Phys. **77**, 5661 (1995).

<sup>31</sup>H. Antoniadis and E. A. Schiff, Phys. Rev. B **46**, 9482 (1992).

<sup>32</sup>J. Isoya, S. Yamasaki, H. Kuchi, A. Matsuda, and K. Tanaka, Phys. Rev. B **47**, 7013 (1993).

<sup>33</sup>H. Branz, Phys. Rev. B **59**, 5498 (1999).

<sup>34</sup>B. Holm, K. B. Nielsen, and B. B. Nielsen, Phys. Rev. Lett. **66**, 2360 (1995).

<sup>35</sup>N. M. Johnson, C. Herring, and C. G. Van de Walle, Phys. Rev. Lett. **73**, 130 (1995).

<sup>36</sup>R. Fisch and D. C. Licciardello, Phys. Rev. Lett. **41**, 889 (1978).

<sup>37</sup>R. Biswas, I. Knon, and C. M. Soukoulis, Phys. Rev. B **44**, 3403 (1991).

<sup>38</sup>Qiming Li and R. Biswas, Phys. Rev. B **52**, 10705 (1995).

<sup>39</sup>E. Tarnow and R. A. Street, Phys. Rev. B **45**, 3366 (1992).

<sup>40</sup>K. Shimizu, T. Tabuchi, M. Iida, and H. Okamoto, J. Non-Cryst. Solids **227/230**, 267 (1998).

<sup>41</sup>R. Biswas, B. C. Pan, and Y. Y. Ye, Phys. Rev. Lett. **88**, 205502 (2002).

<sup>42</sup>S. Pantelides, Phys. Rev. Lett. **58**, 1344 (1987).

<sup>43</sup>R. Biswas and B. C. Pan, Sol. Energy Mater. Sol. Cells **78**, 447 (2003).

<sup>44</sup>F. Yonezawa, S. Sakamoto, and M. Hori, J. Non-Cryst. Solids **137/137**, 135 (1991).

<sup>45</sup>D. Adler, Sol. Cells **9**, 133 (1983).

<sup>46</sup>H. Branz and M. Silver, Phys. Rev. B **42**, 7420 (1990).